Lake surface temperature retrieval from Landsat-8 and retrospective analysis in Karaoun Reservoir, Lebanon

Najwa Sharaf, Ali Fadel, Mariano Bresciani, Claudia Giardino, Bruno J. Lemaire, Kamal Slim, Ghaleb Faour, Brigitte Vinçon-Leite

Lake surface temperature retrieval from Landsat-8 and retrospective analysis in Karaoun Reservoir, Lebanon

Najwa Sharaf
Ali Fadel
Mariano Bresciani
Claudia Giardino
Bruno J. Lemaire
Kamal Slim
Ghaleb Faour
Brigitte Vinçon-Leite

SPIE.

Lake surface temperature retrieval from Landsat-8 and retrospective analysis in Karaoun Reservoir, Lebanon

Najwa Sharaf,[a,b] **Ali Fadel,**[a,*] **Mariano Bresciani,**[c] **Claudia Giardino,**[c]
Bruno J. Lemaire,[b] **Kamal Slim,**[a] **Ghaleb Faour,**[a] **and**
Brigitte Vinçon-Leite[b]

[a]National Council for Scientific Research, National Center for Remote Sensing, Beirut, Lebanon
[b]Laboratoire Eau Environnement Systèmes Urbains, Ecole des Ponts ParisTech, AgroParisTech, Université Paris-Est Créteil, Champs-sur-Marne, France
[c]National Research Council of Italy, Institute for Electromagnetic Sensing of the Environment, Optical Sensing Group, Milano, Italy

Abstract. The importance of lake water surface temperature has long been highlighted for ecological and hydrological studies as well as for water quality management. In the absence of regular field observations, satellite remote sensing has been recognized as a cost-effective way to monitor water surface temperature on large spatial and temporal scales. The thermal infrared sensors (TIRS) onboard of Landsat satellites (since 1984) are adequate tools for monitoring surface temperature of small to medium sized lakes with a biweekly frequency, as well as for performing retrospective analysis. Nonetheless, the satellite data have to deal with effects due to the atmosphere so that several approaches to correct for atmospheric contributions have been proposed. Among these are: (i) the radiative transfer equation (RTE); (ii) a single-channel algorithm that depends on water vapor content and emissivity (SC1); (iii) its improved version including air temperature (SC2); and (iv) a monowindow (MW) algorithm that requires emissivity, atmospheric transmissivity, and effective mean atmospheric temperature. We aim to evaluate these four approaches in a river dammed reservoir with a size of 12 km^2 using data gathered from the band 10 of the TIRS onboard of Landsat 8. Satellite-derived temperatures were then compared to *in situ* data acquired from thermistors at the time of Landsat 8 overpasses. All approaches showed a good performance, with the SC1 algorithm yielding the lowest root mean square error (0.73 K), followed by the SC2 method (0.89 K), the RTE (0.94 K), and then the MW algorithm (1.23 K). Based on the validation results, we then applied the SC1 algorithm to Landsat 4, 5, and 8 thermal data (1984 to 2018) to extend data series to past years. These data do not reveal any warming trend of the reservoir surface temperature. The results of this study also confirm how the 100-m spatial resolution of TIRS is valuable as an additional source of data to field-based monitoring. © *2019 Society of Photo-Optical Instrumentation Engineers (SPIE)* [DOI: 10.1117/1.JRS.13.044505]

Keywords: water surface temperature; reservoir; remote sensing; Landsat; thermal infrared sensor.

Paper 190433 received Jun. 7, 2019; accepted for publication Sep. 25, 2019; published online Oct. 24, 2019.

1 Introduction

Lake water temperature is a key parameter influencing the functioning of freshwater ecosystems. Gaining insight about the distribution of water surface temperature is crucial for understanding the hydrodynamic functioning and biological processes in lakes and reservoirs.[1,2]

Conventional methods for water surface temperature measurements, which make use of thermistors on buoys and radiometry, might benefit from additional data from remote sensing, providing a larger spatial coverage of water characteristics over time. Coarse-spatial high-frequency satellite sensors [e.g., the advanced very high-resolution radiometer and the moderate resolution imaging spectroradiometer (MODIS)] have been commonly used to map medium to

---

large lakes worldwide,[3,4,5] as well as to develop time-series to assess the lake sensitivity to global change.[6,7] As the spatial resolution of these sensors might be too coarse for mapping water surface temperature in smaller lakes or reservoirs, sharpening techniques or higher spatial resolution sensors have been alternatively used. For example, Teggi[8] developed an algorithm for improving the spatial resolution of ASTER from 90 to 30 m to map water surface temperature in coastal waters and of watercourses, whereas other studies made use of Landsat imagery.[9,10,11]

In particular, although with at around biweekly revisiting time, Landsat 4 and 5 TM (thematic mapper, 1984 to 2013, spatial resolution of the thermal band 120 m), Landsat 7 ETM+ (enhanced thematic mapper, since 1999, spatial resolution of the thermal band 60 m), and the most recent Landsat 8 TIRS (thermal infrared sensor, since 2013, spatial resolution of the thermal band 100 m) have the appropriate spatial resolution for mapping medium to small size waterbodies. Since the Landsat Data Continuity Mission program holds an impressive continuous record of 45 years of imagery data at an approximately biweekly revisiting time, Landsat is a prime platform for retrospective studies on thermal properties of inland waters.

Owing to the trade-off between spatial and temporal resolutions, several techniques (data fusion or disaggregation) have been developed to derive surface temperature at high spatial and temporal resolutions from existing remote sensing data.[12] These approaches generate data with fine spatial resolution and temporal frequency by combining multisensor spatial and temporal characteristics. Most of them were used for land surface temperature retrieval,[13] whereas their application to inland waters is very scarce. Examples of these techniques include the fusion of Landsat 8 panchromatic and thermal infrared images to enhance the spatial resolution of the latter[14] and disaggregating surface temperature from MODIS images to the Landsat spatial resolution using Landsat visible-near-infrared data.[15] Yet, the models or algorithms implicated in these techniques require additional validation and improvement.[16]

In order to obtain accurate and comparable measurements of water surface temperature from spaceborne observations, atmospheric corrections accounting for atmospheric attenuation and emission should be undertaken for each image. Several approaches have been proposed to correct for atmospheric contributions. One way to correct these contributions is to apply directly the radiative transfer equation (RTE), which requires atmospheric parameters including transmissivity and downwelling and upwelling radiances.[17,18] The method has been successfully applied to characterize the impact of river plumes in marine waters during a significant flood event.[19]

Another way is to use its approximation, the generalized single-channel algorithm (SC1) developed by Jiménez-Muñoz and Sobrino[20] and further improved (SC2) in Cristóbal et al.[21] or the monowindow (MW) algorithm[22] by Qin et al.[23] and Isaya Ndossi and Avdan.[24] The SC1 algorithm reduces the need for local data to atmospheric water vapor content and emissivity. However, an error in water vapor content or values outside its validity range (>3 g cm^2) might increase the errors in retrieving surface temperature. The SC1 algorithm can be applied to any thermal infrared sensor. It was mostly used for surface temperature retrieval over land[24] while few studies dealt with direct applications to inland waters.[25,26] Furthermore, it was more often validated for Landsat 4, 5, and 7 than for Landsat 8, which is the most recent.

Because the SC1 algorithm only depends on water vapor content and emissivity, Cristóbal et al.[21] proposed an improved version of the SC1 algorithm, hereafter denoted as the SC2 algorithm, in order to minimize the errors associated with the amount of water vapor content. The SC2 algorithm has a supplementary input, near-surface air temperature. It operates on a wider range of water vapor content and air temperature and was evaluated for Landsat 8 TIRS.

The MW algorithm has been used for retrieving surface temperature from the thermal bands of Landsat sensors (TM, ETM+, and TIRS). Similar to the RTE, the SC1, and SC2 algorithms, the MW algorithm requires atmospheric parameters including emissivity, atmospheric transmissivity, and effective mean atmospheric temperature.

The launch of Landsat 8 with two thermal bands (band 10: 10.6 to 11.19 μm and band 11: 11.5 to 12.51 μm) allowed the application of split-window algorithms that have been developed for decades[27] to correct satellite data acquired with multiple bands in the thermal infrared wavelengths. Unfortunately, due to the calibration uncertainties in band 11, it is not recommended that band 11 be used for the split-window technique (USGS-Landsat Mission 2017 (Ref. [28])], which is why single-channel algorithms (also called MW algorithms) using band 10 are more appropriate for surface temperature estimation.[29]

The aims of this work are: (1) to assess the performance of four approaches, namely, RTE, MW, SC1, and SC2 for retrieving surface water temperature in a river dammed reservoir in a semiarid climate and (2) to look for a trend in the mean temperature at the water surface. The site is Karaoun Reservoir, located in Lebanon and considered to be an altered ecosystem affected by several anthropogenic activities.[30] The RTE and the MW, SC1, and SC2 algorithms were applied to a set of Landsat 8 images acquired in 2016 and 2017 using band 10 of the TIRS and compared to subsurface temperature observations. After validation, the most effective approach was used to assess retrospective water surface temperatures (1984 to 2015 and 2018) from the Landsat 4 and 5 TM and Landsat 8 TIRS sensors.

2 Materials and Methods

2.1 Study Site

The largest freshwater body in Lebanon, Karaoun Reservoir (Fig. 1, 33°34'N, 35°41'E), is deep, monomictic, and eutrophic, and belongs to the few regularly monitored lakes and reservoirs of the Middle East. It has a surface area of 12 km^2 at full capacity, maximum and mean depths of 60 and 19 m, respectively.[31] Karaoun Reservoir serves different purposes, such as power generation and irrigation, leading to large fluctuations in its water level (about 25 m in a year), which is also influenced by the hydrological cycle. These cause considerable variations in the water surface temperatures and in the stratification pattern.[32] During the dry season, the reservoir stratifies over a considerable period between May and August. The thermal stratification is then broken down as a result of vertical mixing due to air cooling and higher inflows. Monitoring of water temperature was mainly performed on a single point S_D near the dam in 2016.[33] With no measurements available on a spatial scale (except for 2017) and given the effect of water temperature on its biota distribution,[34] synoptic estimations of water surface temperature are valuable for this ecosystem.

2.2 Radiative Transfer Equation

For a single infrared thermal band, the at-sensor radiance can be approximated based on the RTE according to the following expression:[35]

$$L_{\text{sen}} = \tau[\varepsilon L_\lambda(T_{\text{RTE}}) + (1 - \varepsilon)L_d] + L_u, \tag{1}$$

where L_{sen} (in $\text{W m}^{-2}\,\text{sr}^{-1}\,\mu\text{m}^1$ is the radiance measured by the TIRS (or top of atmosphere radiance), τ is the atmospheric transmissivity, ε is the emissivity of water, $L_\lambda(T_{\text{RTE}})$ represents
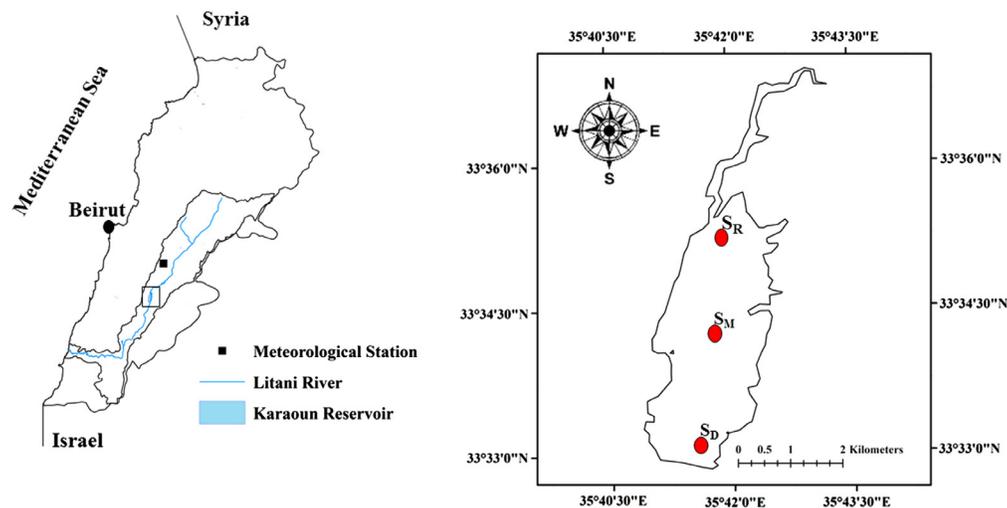

Fig. 1 Location of Karaoun reservoir with the sampling locations S_D near the dam, S_M in the middle of the reservoir, and S_R near the Litani River inlet.

Planck's function of a blackbody at surface temperature T_{RTE}, L_d is the downwelling atmospheric radiance, and L_u is the upwelling atmospheric radiance.

Surface temperature (T_{RTE}) can be then calculated from Eq. (2) as follows:

$$T_{RTE} = \frac{K_2}{\ln\left[\frac{K_1}{L_\lambda(T_{RTE})} + 1\right]}, \tag{2}$$

where (T_{RTE}) is the surface temperature in K, K_1 and K_2 are the calibration parameters for TIRS band 10, their values are 774.8853 W m^{-2} sr^{-1} μm^{-1} and 1321.0789 K, respectively. T_{RTE}, hereafter, designates surface temperature retrieved from the RTE.

Using the TIRS band 10, García-Santos et al.[36] found a lowest root mean square error (RMSE) of 2.3 K with the RTE. Furthermore, Yu et al.[37] used the RTE for retrieving land surface temperature at four study sites in the United States and found that the RMSE between estimated and ground temperature measurements was much higher with TIRS band 11 (1.17, 1.19, 1.12, and 0.75 K) than with TIRS band 10 (0.87, 1.01, 0.93, and 0.57 K).

2.3 General Single-Channel Algorithm

The general SC1 algorithm for retrieving surface temperature was initially proposed by Jiménez-Muñoz and Sobrino.[20] The algorithm aims at retrieving surface temperature in a more operational way than using the RTE. It depends only on water vapor w and emissivity ε as input. Hence, it avoids dependence on atmospheric parameters such as atmospheric transmissivity τ and upwelling and downwelling atmospheric radiances L_u and L_d, which are rarely available and somewhat difficult to measure.

The SC1 algorithm retrieves surface temperature (T_{SC1} in K) using the following general equation:

$$T_{SC1} = \gamma[\varepsilon^{-1}(\Psi_1 L_{sen} + \Psi_2) + \Psi_3] + \delta. \tag{3}$$

γ and δ are expressed as

$$\gamma \approx \frac{T_{sen}^2}{b_\lambda \times L_{sen}}; \delta \approx T_{sen} - \frac{T_{sen}^2}{b_\lambda}, \tag{4}$$

where T_{sen} is the at-sensor brightness temperature in K, b_λ is equal to 1324 K for Landsat 8 TIRS band 10, 1290 K for Landsat 4 band 6, and 1256 K for Landsat 5 band 6, and Ψ_1, Ψ_2, and Ψ_3 are the atmospheric functions.

The concept of the SC1 algorithm aims at the approximation of the atmospheric functions presented in Eq. (3) versus the water vapor content (w in g cm^{-2}) through a polynomial fit. In a matrix notation, this approximation can be expressed as follows, where the coefficients C_{ij} (Sec. 5) are obtained by simulation from the sensor filter response:

$$\begin{pmatrix} \Psi_1 \\ \Psi_2 \\ \Psi_3 \end{pmatrix} = \begin{pmatrix} C_{11} & C_{12} & C_{13} \\ C_{21} & C_{22} & C_{23} \\ C_{31} & C_{32} & C_{33} \end{pmatrix} \begin{pmatrix} w^2 \\ w \\ 1 \end{pmatrix}. \tag{5}$$

A particular set of coefficients linking transmissivity and radiances to the water vapor content was derived from the filter response of Landsat 5 TM. This algorithm was further revised by Jiménez-Muñoz et al.[38] and sets of coefficients were proposed for Landsat 4 and 7. Eventually new sets of coefficients for Landsat 8 TIRS were provided by Jiménez-Muñoz et al.[39] Ψ_1, Ψ_2, and Ψ_3 are the atmospheric functions given by

$$\Psi_1 = \frac{1}{\tau}, \Psi_2 = -L_d - \frac{L_u}{\tau}, \quad \text{and} \quad \Psi_3 = L_d. \tag{6}$$

Recently, Cristóbal et al.[21] further introduced air temperature to the algorithm together with water vapor content (w) as it is supposed to improve to the algorithm's performance.

The atmospheric functions are then fitted with a second degree polynomial based on water vapor content (w) and near surface air temperature (T_0) in K as follows:

$$\Psi_n = iw^2 + hT_0^2 + gw + fT_0 + eT_0^2 w + dT_0 w + cT_0 w^2 + bT_0^2 w^2 + a, \qquad (7)$$

where $n = 1, 2, 3$ and $a, b, c, d, e, f, g, h, i$ are the numerical coefficients of the statistical fit (Sec. 5). In this case, surface temperature (T_{SC2}) is retrieved from Eq. (3).

Within the general SC1 algorithm, the approximations of the atmospheric functions differ for Landsat 4, 5, and 8 and each case is assigned a different set of coefficients (Sec. 5). For a complete description, readers are advised to refer to Jiménez-Muñoz et al.[38,39] The SC1 algorithm was implemented as follows: γ and δ were calculated from Eq. (4), the atmospheric functions Ψ_1, Ψ_2, and Ψ_3 were obtained from Eq. (5) after selection of appropriate coefficients for the TM and the TIRS sensors and assigning the corresponding w values. Once all parameters were calculated, surface temperature (T_{SC1}) with atmospheric coefficients calculated from Eq. (5) was then retrieved using Eq. (3) with a value of 0.995 for water emissivity. The SC2 algorithm was implemented in the same manner. The atmospheric functions were obtained from Eq. (7) after assigning specific coefficients for each. Surface temperature (T_{SC2}) was then retrieved from Eq. (3).

A long-term change in air temperature is expected to cause a simultaneous change in surface water temperatures of lakes. Schneider and Hook[40] demonstrated that surface water temperature of inland water bodies increases more rapidly than air temperature worldwide. As a result, air temperature has been used in several modeling approaches as a predictor of lake surface temperature.[41,42] The most recent SC2 algorithm developed with water vapor content and air temperature has not been yet validated as extensively as the SC1 approach. It has been shown to yield a RMSE of the order of 1 K against *in situ* data recorded over an area containing a variety of vegetation and snow in Alaska.[21]

Both the SC1 and SC2 approaches are expected to provide good results. The choice of the method depends on the range of water vapor content. The good performance of the former is still limited to values >3 g cm^{-2}. Hence, errors are expected to increase with the amount and errors associated with the water vapor content. On the contrary, the SC2 approach shows a superior performance in a wide range of water vapor content and air temperature.

2.4 Monowindow Algorithm

The MW algorithm, initially developed by Qin et al. [23] and widely used for surface temperature retrieval from Landsat TM and ETM$^+$ single thermal bands, depends on emissivity, atmospheric transmissivity, and effective mean atmospheric temperature. Isaya Ndossi and Avdan[24] further improved the algorithm for surface temperature retrieval from Landsat 8 TIRS band 10 by including local meteorological data for estimating the effective mean atmospheric temperature.

Surface temperature can be retrieved from the MW algorithm in the following form:

$$T_{MW} = \frac{a_{10}(1 - C_{10} - D_{10}) + [b_{10}(1 - C_{10} - D_{10}) + C_{10} + D_{10}]T_{sen} - D_{10}T_a}{C_{10}}, \qquad (8)$$

where T_{MW} is the surface temperature retrieved from band 10 of the TIRS, a_{10} and b_{10} are the constants used to approximate the derivative of the Planck radiance function for the TIRS band 10 and depend on the range of T_{sen} (here $a_{10} = -62.7182$ and $b_{10} = 0.4339$), T_a is the effective mean atmospheric temperature in K, and C_{10} and D_{10} are the internal parameters for the algorithm:

$$C_{10} = \tau\varepsilon, \qquad (9)$$

$$D_{10} = (1 - \tau)[1 + (1 - \varepsilon)\tau]. \qquad (10)$$

As before, τ and ε are, respectively, atmospheric transmissivity derived from the TIRS band 10 spectral response curve and water emissivity.

The effective mean atmospheric temperature is approximated from the near surface air temperature T_0 (from a ground meteorological station) from the following linear relation for an atmosphere of mid-latitude summer:[23]

$$T_a = 16.0110 + 0.9262T_0. \tag{11}$$

The MW algorithm was shown to provide lower discrepancies than the SC1 algorithm, with RMSEs of 0.84 and 1.05 K, respectively, using TIRS band 10.[23] Yet, Sobrino et al.[43] compared the MW and SC1 approaches using thermal data from the TM band 6 and found that the SC1 algorithm yielded less errors than the MW algorithm with root mean square deviations of 1 and 2 K, respectively.

The performance of the algorithms was assessed by estimating the RMSE, the mean absolute error (MAE), and the Pearson correlation coefficient (r) between observed ($T_{in\,situ}$) and satellite-derived water surface temperatures from the RTE, SC1, SC2, and MW algorithms (T_{RTE}, T_{SC1}, T_{SC2}, and T_{MW}).

2.5 Data Collection

19 cloud free Landsat 8 scenes corresponding to a total of 31 water surface temperature observations ($T_{in\,situ}$) were acquired every 16 days (at 11:10 a.m. local time) from May 15 to October 16, 2016, and from April 26 to September 1, 2017. Due to variations in the water level, the surface of the reservoir was extracted for each scene, using the normalized difference water index.[44]

Continuous *in situ* water surface temperature data were available for both years and were extracted at the time of satellite overpasses. Measurements were recorded with a thermistor at 0.5-m depth at a single-location S_D near the dam in 2016, and at 0.2-m depth at three points in 2017, S_D, S_M in the middle of the reservoir, and S_R near the Litani River inlet (Fig. 1). In the literature, the bulk surface temperatures that are used to assess satellite inferred observations are usually measured over depths ranging from a few centimeters to several meters.[2]

In addition to 2016–2017 images, 153 images from the Landsat 4 and 5 TM and Landsat 8 TIRS sensors were used to characterize the evolution of water surface temperature between 1984–2015 and 2018, whereas no *in situ* water temperature records were available for this period. Thermal infrared data were freely downloaded from the United States Geological Survey. Images were converted from digital numbers to at-sensor radiance L_{sen} and at-sensor brightness temperature T_{sen} by means of the ENVI software (version 5.2) using calibration parameters from the metadata file.

For the RTE and the MW algorithms, atmospheric parameters (τ, L_u, and L_d) were computed with the atmospheric correction parameter calculator of the National Center for Environmental Prediction (NCEP)[17,35] using the Landsat 8 TIRS band 10 spectral response curve. This atmospheric correction tool uses the NCEP modeled atmospheric global profiles and the moderate resolution atmospheric transmission radiative transfer code. Daily water vapor content was collected for the whole validation period and downloaded from the ERA interim dataset of the European Centre for Medium-Range Weather Forecasts at 12:00 p.m.[45] Near surface air temperature T_0 used for both the SC2 and MW algorithms was taken from a meteorological ground station (Tal-Amara meteorological station, Fig. 1) although if it had been available it could have been taken from atmospheric radiosoundings.

3 Results and Discussion

In order to validate surface temperature retrieval, we compared observed water surface temperatures to estimates by the RTE, SC1, SC2, and the MW algorithms. The results are summarized in Fig. 2. The values of the statistical indicators suggest a good agreement between measurements and estimations of surface temperatures. Very high correlations were obtained with the four approaches (Table 1). With $r = 0.97$ for T_{SC1} and 0.96 for T_{SC2}, the SC1 and SC2 methods showed the highest correlations and least errors. The SC1 and SC2 algorithms yielded RMSEs of 0.73 and 0.89 K and MAEs of 0.71 and 0.88 K, respectively. The RTE also performed well,
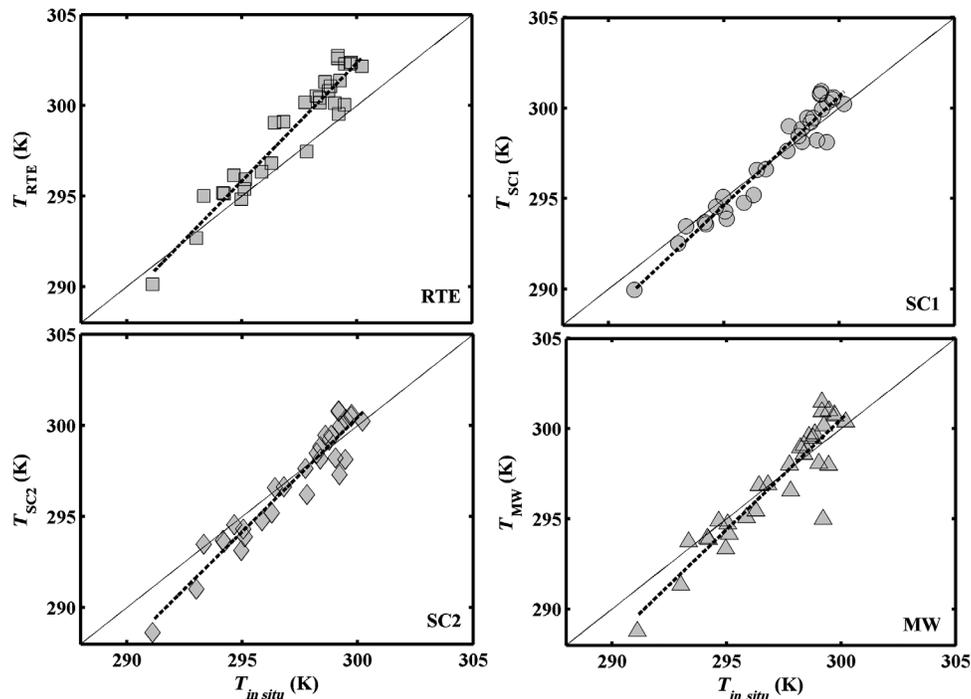
Fig. 2 Temperature measurements ($T_{in\,situ}$) in 2016 and 2017 versus corrected Landsat 8 TIRS band 10 data (T_{RTE}, T_{SC1}, T_{SC2}, and T_{MW}), respectively, from the RTE, the SC1, the SC2, and the MW algorithms ($n = 31$) with the following equations: $y_{RTE} = 1.31x - 88.9$, $y_{SC1} = 1.2x - 60.6$, $y_{SC2} = 1.26x - 77.11$, $y_{MW} = 1.23x - 67.1$.

Table 1 Pearson correlation coefficient r; root mean squared error, RMSE (K); and mean absolute error, MAE (K), between field measurements ($T_{in\,situ}$) and estimations from the RTE (T_{RTE}), the SC1, and SC2 algorithms (T_{SC1} and T_{SC2}) and the MW algorithm (T_{MW}).

	r	RMSE (K)	MAE (K)
T_{RTE}	0.95	0.94	1.6
T_{SC1}	0.97	0.73	0.71
T_{SC2}	0.96	0.89	0.88
T_{MW}	0.92	1.23	1.01

however, with a bias as seen on its MAE of 1.6 K and an RMSE of 0.94 K. The MW algorithm displayed the weakest results with an RMSE and a MAE of 1.23 and 1.01 K, respectively.

Further, the RMSE values observed in each approach agree with values found in similar validation studies[25,46] over reservoirs. For the SC1 algorithm for instance, Jiménez-Muñoz et al.,[39] whose estimations were validated with simulated data selected over land, obtained RMSEs around 1.5 K only when the water vapor content is lower than 3 g cm^{-2}. In this study, RMSE is 0.73 K but the water vapor content remained in the range where the SC1 algorithm performs best. For a more humid atmosphere, RMSEs could reach up to 5 K when using the SC1 algorithm.[39]

Among the four approaches, the SC1 algorithm gave the highest correlations and lowest RMSE and MAE in this study. Based on these results and as long as the water vapor content is in the recommended range, the SC1 algorithm is the preferable method for estimating surface temperature from TIRS band 10 at Karaoun Reservoir. Unlike the RTE and the MW algorithm, it minimizes the input of atmospheric parameters and thus the errors are mostly restricted to the accuracy of the water vapor content.
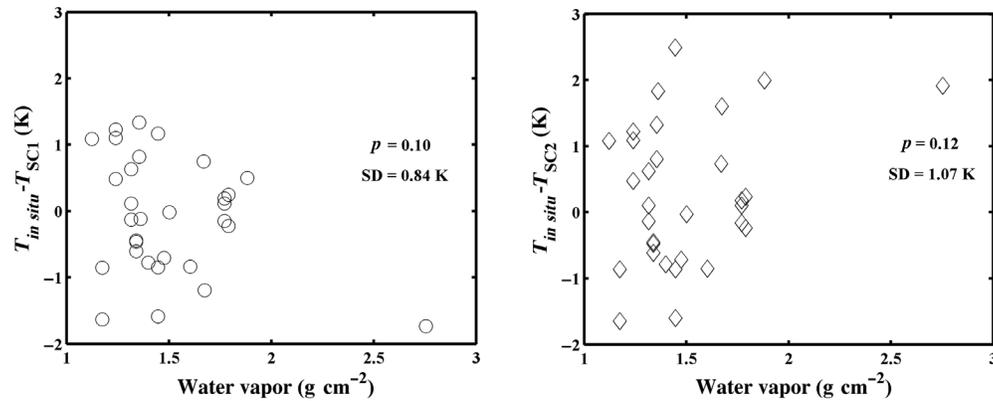
Fig. 3 Difference of *in situ* and surface temperatures in 2016 and 2017 as a function of the water vapor content, $n = 31$.

Figure 3 shows the difference between *in situ* water surface temperatures and estimates from the SC1 and SC2 algorithms plotted versus the water vapor content. The water vapor content ranges from 1 to 3 $\mathrm{g\,cm^{-2}}$. The difference between $T_{in\,situ}$ and T_{SC1} exhibits no trend with the water vapor content ($p = 0.10$). The range of differences exceeds the -1 K to 1 K interval (standard deviation SD is 0.84 K). This range is consistent with literature results.[21] Although García-Santos et al.[36] observed an increase in the errors with the water vapor content, the lack of trend here can be attributed to its small range, with few points at high values.

The differences are slightly higher for the SC2 algorithm with a standard deviation of 1.07 K and some differences above 2 K. Cristóbal et al.[21] reported better estimations and less bias with the SC2 algorithm: their errors tended to be within the -1 K to 1 K range. However, they also reported that the performance of the SC2 algorithm and hence the expected errors can differ between different types of study sites. For example, they found that the SC2 algorithm performed better over vegetation than snow, which can be due to emissivity. These findings call for additional validation studies over inland waterbodies where, in comparison to land, the performance of such algorithms was seldom assessed.

A difference of a few degrees can be observed between satellite derived skin temperatures and *in situ* bulk water temperatures.[11,47] Most often, skin temperatures are cooler than bulk temperatures. This is called the cool skin effect[48] although other sources of mismatch might explain this difference (e.g., the thermal emission by adjacent targets).

Validating satellite-derived surface temperatures is quite a challenge as atmospheric conditions can greatly influence the accuracy of the process, whereas the timing and the depth at which water surface temperature is measured *in situ* might not be directly comparable to satellite estimations. The main error sources in surface temperature retrieval associated with the SC1 algorithm arise from atmospheric effects and surface emissivity uncertainties. This algorithm requires only water vapor content and surface emissivity. Unfortunately, these variables have never been measured at Karaoun Reservoir. The fact that these variables are obtained through modeling or approximations makes it, to a certain degree, difficult to obtain minimal discrepancies between remote sensing estimations and ground observations. As for *in situ* surface temperatures, they were recorded simultaneously with the Landsat 8 overpasses for all dates, thus avoiding another source of uncertainty. Measurements of *in situ* bulk temperatures were recorded at 50 and 20 cm below the surface, whereas satellite-derived temperatures are provided at the top millimeter of the water surface layer. Differences between the measurement depth of lake *in situ* and satellite surface temperature estimations are neglected since measurements have been shown to be representative of satellite-derived surface temperatures, at least during morning overpasses (11:10 a.m.).[49]

Using the SC1 algorithm, we then proceeded with the water surface temperature retrieval from band 6 and band 10 of the Landsat TM and TIRS, respectively, between 1984 and 2015 and in 2018 using 153 cloud free images. Water temperature was averaged over the reservoir surface. Between 1984 and 2018, remote sensing estimations did not indicate a significant warming trend with a very high p value of 0.9 for the whole data series. During that period,
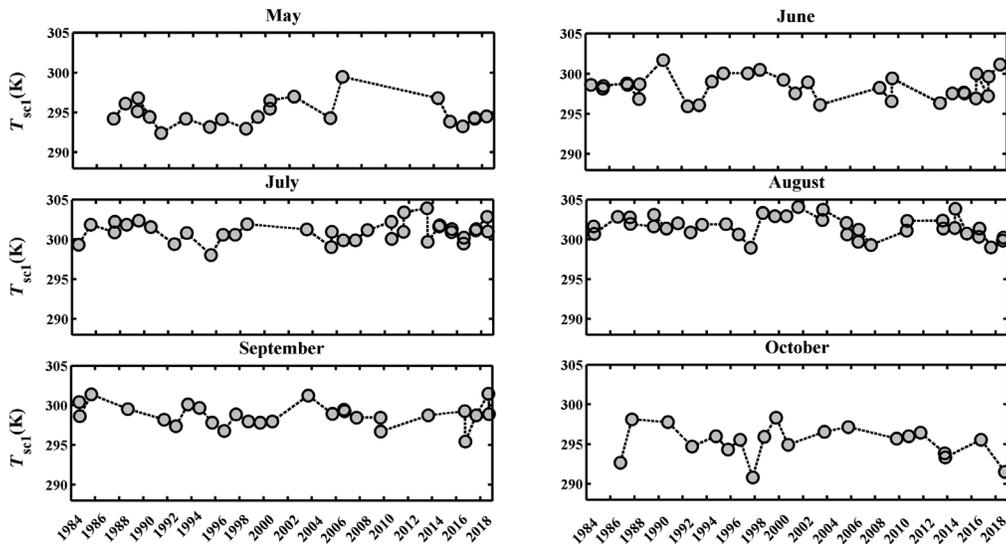
Fig. 4 Surface-averaged water temperature (T_{SC1}) between 1984 and 2018 derived from Landsat 4, 5, and 8.

surface temperature ranged between 290 and 304 K with the latter, highest temperature, being recorded in August of 2001. According to each month of the year, the highest temperatures were found in the following years; 2006 for May, 1990 for June, 2013 for July, 2001 for August, 1985 for September, and 1999 for October (Fig. 4). Moreover, there is no significant trend in the surface temperatures sorted by month in the year.

Deutsch and Alameddine[50] conducted a retrospective study of water surface temperature over Karaoun Reservoir between 1984 and 2015 and did not find a significant warming trend except in August. They initially applied the SC1 algorithm to the period 2000 to 2015. However, instead of using water vapor content to calculate the atmospheric functions and thus avoid the use of several atmospheric parameters, they adopted τ, L_u, and L_d from NCEP data as input to the algorithm. They also found that between 2000 and 2015 brightness temperatures derived from Landsat sensors were in better correlation with *in situ* measurements of surface temperature than with the atmospherically corrected estimates. This further led to their use of brightness temperature and *in situ* measurements to develop a linear regression model and derive data prior to 2000, in order to ultimately analyze the surface temperature trend between 1984 and 2015. The use of three atmospheric parameters (τ, L_u, and L_d) as input to the SC1 algorithm and brightness temperature data instead of atmospherically corrected surface temperatures could add uncertainty in surface temperature retrieval.[36] With reference to the historical analysis of surface temperature at Karaoun Reservoir, this can also explain the difference between the findings of Deutsch and Alameddine[50] and this work, in which a warming trend of surface temperature was not discernable between 1984 and 2018 after applying the SC1 algorithm in its original form, namely with water vapor data and emissivity as only inputs.

Surface temperatures of inland waterbodies have been used as indicators of climate change.[6] Yet such studies are still limited, due to the lack in long-term measurements, and focus on waterbodies greater than 500 km^2,[40] thus neglecting small to medium sized lakes and reservoirs.

Some of the climate-induced changes to lake physical properties are manifested by higher water surface temperatures, the earlier onset and longer periods of thermal stratification and overall greater lake stability.[51–54] These manifestations have been largely attributed to meteorological forcing and morphometry. Although it is commonly considered and shown that lake and reservoir water temperature will warm in synchrony with increasing air temperatures,[55] the latter is not always reflected in long-term temperature trends in reservoirs.[56] The thermal dynamics differ between lakes and reservoirs. Reservoirs experience large fluctuations in the water level, often irregular over the years due to operational constraints, and thus thermal dynamics are expected to be more variable in contrast to many lakes where the water volume does not change

significantly and the seasonal heat dynamics dominates. Therefore, the fact that the conditions at Karaoun Reservoir are not seasonally reproducible might have disabled the possibility to detect a warming trend of surface temperature although the influence of other climatic factors should not be excluded.

Studies dealing with warming trends of lake and reservoir surface temperature in the Middle East are scarce except for Lake Kinneret, Israel. The analysis of the surface temperature record (1984 to 2018) of Karaoun Reservoir contrasts the trend found at Lake Kinneret, which revealed a warming (~0.036°C per year) of lake summer surface temperature between 1969 and 2015.[57] However, the increase in water temperature at Lake Kinneret was mainly attributed to anthropogenic activities such as the reduction in the water level while climate change had a minor influence.[58]

Water surface temperature is a key parameter for determining ecological processes in lakes and reservoirs as it influences biological processes such as the primary productivity. In lake Dianchi, China, surface water temperature was found to be the main cause of algal bloom development.[1] At Karaoun Reservoir blooms of toxic species of cyanobacteria have occurred annually since 2009.[28] Between 1984 and 2007, a recent study making use of a remote sensing algorithm to derive concentrations of the phycocyanin pigment demonstrated the occurrence of cyanobacteria at Karaoun Reservoir.[59] Concentrations were found to be significantly high (>50 μg/L) with a peak of phycocyanin concentration occurring in May of 2006 thus coinciding with the highest temperature recorded in May between 1984 and 2018 as shown in this work.

Acquiring a long-term record of water quality parameters is valuable especially in Middle Eastern areas where lakes and reservoirs are poorly monitored. The record of water surface temperature found in this work is an additional source of data, which can complement *in situ* observations and interpolate temporal gaps. Water surface temperature data can also have implications for reservoir management through environmental applications. It reflects the impact of climate change, stratification, and mixing. Further, it can also be used to understand the hydrological cycle and verify hydrodynamic models.

4 Conclusions and Perspectives

Water surface temperature is an important parameter in limnological studies. Several algorithms have been developed to retrieve surface temperature from thermal bands of the long series of Landsat. Nevertheless, validation studies are still useful to assess the effectiveness of algorithms applied to satellite data when applied to a new case study.

In this work, we validated against *in situ* measurements water surface temperature estimated with four single-channel approaches applied to data acquired by the TIRS (band 10) onboard of the latest Landsat 8.

The results on method comparison showed a good agreement between *in situ* observations and satellite estimations for all four approaches. In particular, the SC1 algorithm provided the lowest errors in terms of RMSE (0.73 K) and MAE (0.71 K) followed by the SC2 algorithm and the RTE. The MW algorithm had the weakest performance and yielded the highest RMSE (1.23 K). Further, the historic retrieval of the reservoir surface temperature between 1984 and 2018 did not reveal a warming trend.

We conclude that the SC1 algorithm is the most adequate for achieving the finest match with field-based temperature observations for Karaoun Reservoir. The results indicate that the algorithm, which was formerly mostly validated on land, is also suitable for retrieving the water surface temperature of medium to small lakes and reservoirs in semiarid regions.

However, additional validation studies are still needed to extent the analysis to other inland waterbodies at different latitudes and with different thermal regimes. The results of this analysis might help to exploit the use of Landsat in lake surface water monitoring and hence to overcome limitations imposed by conventional measurement methods. These results can further serve for hydrodynamic modeling studies where synoptic observation of lake surface water during time might be used for initializing the model or for validating model simulations of water surface temperature.

5 Appendix: Numerical Coefficients of the General Single-Channel Algorithm

The atmospheric functions of TIRS band 10 presented in Eq. (5) and included in the SC1 algorithm were calculated from a second-order polynomial fit with the following coefficients:[39]

$$
\begin{pmatrix} \Psi_1 \\ \Psi_2 \\ \Psi_3 \end{pmatrix} = \begin{pmatrix} 0.040 & 0.0292 & 1.02 \\ -0.383 & -1.50 & 0.20 \\ 0.00918 & 1.36 & -0.275 \end{pmatrix} \begin{pmatrix} w^2 \\ w \\ 1 \end{pmatrix}. \tag{12}
$$

The coefficients for the atmospheric functions of the thermal band 6 of Landsat 4 and 5 are shown in Table 2 following the matrix notation expressed in Eq. (5).

Table 2 Coefficients of the atmospheric functions for band 6 of Landsat 4 and Landsat 5.[38]

Platform	C_{ij}	$i = 1$	$i = 2$	$i = 3$
Landsat 4 band 6	$j = 1$	0.0877	−0.0967	1.09
	$j = 2$	−0.703	−0.612	−0.122
	$j = 3$	−0.0252	1.51	−0.488
Landsat 5 band 6	$j = 1$	0.106	−0.130	1.12
	$j = 2$	−0.814	−0.476	−0.291
	$j = 3$	−0.0442	1.62	−0.487

The numerical coefficients for the atmospheric functions of TIRS band 10 shown in Eq. (7) are presented in Table 3.

Table 3 Numerical coefficients for the atmospheric functions of TIRS band 10 listed in Eq. (7).[21]

Coefficients	Ψ_1	Ψ_2	Ψ_3
a	4.47	−30.4	−3.76
b	−0.0000748	0.000911	−0.000141
c	0.0466	−0.573	0.0911
d	0.0232	−0.784	0.545
e	−0.0000496	0.00140	−0.000909
f	−0.0263	0.215	0.0418
g	−2.45	106	−80.0
h	0.0000492	−0.000376	−0.000104
i	−7.21	89.6	−14.7

Acknowledgments

References

1. K. Yang et al., "Spatial and temporal variations in the relationship between lake water surface temperatures and water quality-A case study of Dianchi Lake," *Sci. Total Environ.* **624**, 859–871 (2018).
2. S. R. Schmidt et al., "Temporal and spatial scales of water temperature variability as an indicator for mixing in a polymictic lake," *Inland Waters* **8**(1), 82–95 (2018).
3. D. C. Oesch et al., "Lake surface water temperature retrieval using advanced very high resolution radiometer and moderate resolution imaging spectroradiometer data: validation and feasibility study," *J. Geophys. Res-Oceans* **110**(C12), 1–17 (2005).
4. A. Reinart and M. Reinhold, "Mapping surface temperature in large lakes with MODIS data," *Remote Sens. Environ.* **112**, 603–611 (2008).
5. C. Giardino et al., "Application of remote sensing in water resource management: the case study of Lake Trasimeno, Italy," *Water Resour. Manag.* **24**(14), 3885–3899 (2010).
6. C.M. O'Reilly et al., "Rapid and highly variable warming of lake surface waters around the globe," *Geophys. Res. Lett.* **42**(24), 10–773 (2015).
7. S. Pareeth et al., "Warming trends of perialpine lakes from homogenised time series of historical satellite and in-situ data," *Sci. Total Environ.* **578**, 417–426 (2017).
8. S. Teggi, "A technique for spatial sharpening of thermal imagery of coastal waters and of watercourses," *Int. J. Remote Sens.* **33**(10), 3063–3089 (2012).
9. C. Giardino et al., "Detecting chlorophyll, Secchi disk depth and surface temperature in a sub-alpine lake using Landsat imagery," *Sci. Total Environ.* **268**(1–3), 19–29 (2001).
10. C. Wloczyk et al., "Sea and lake surface temperature retrieval from Landsat thermal data in Northern Germany," *Int. J. Remote Sens.* **27**(12), 2489–2502 (2006).
11. Y. Huang et al., "Analysis of thermal structure of arctic lakes at local and regional scales using in situ and multidate Landsat-8 data," *Water Resour. Res.* **53**(11), 9642–9658 (2017).
12. W. Zhan et al., "Disaggregation of remotely sensed land surface temperature: literature survey, taxonomy, issues, and caveats," *Remote Sens. Environ.* **131**, 119–139 (2013).
13. V. M. Bindhu et al., "Development and verification of a non-linear disaggregation method (NL-DisTrad) to downscale MODIS land surface temperature to the spatial scale of Landsat thermal data to estimate evapotranspiration," *Remote Sens. Environ.* **135**, 118–129 (2013).
14. H. S. Jung and S. W. Park, "Multi-sensor fusion of Landsat 8 thermal infrared (TIR) and panchromatic (PAN) images," *Sensors* **14**(12), 24425–24440 (2014).
15. M. Bisquert et al., "Evaluation of disaggregation methods for downscaling MODIS land surface temperature to Landsat spatial resolution in Barrax test site," *IEEE J. Sel. Top. Appl. Earth Obs. Remote Sens.* **9**(4), 1430–1438 (2016).
16. B. Chen et al., "Comparison of spatiotemporal fusion models: a review," *Remote Sens.* **7**(2), 1798–1835 (2015).
17. J.A. Barsi et al., "Validation of a web-based atmospheric correction tool for single thermal band instruments," *Proc. SPIE* **5882**, 58820E (2005).
18. J. Barsi et al., "Landsat-8 thermal infrared sensor (TIRS) vicarious radiometric calibration," *Remote Sens.* **6**(11), 11607–11626 (2014).
19. V. E. Brando et al., "High-resolution satellite turbidity and sea surface temperature observations of river plume interactions during a significant flood event," *Ocean. Sci.* **11**(6), 909–920 (2015).
20. J. C. Jiménez-Muñoz and J. A. Sobrino, "A generalized single-channel method for retrieving land surface temperature from remote sensing data," *J. Geophys. Res. Atmos.* **108**(D22) (2003).

21. J. Cristóbal et al., "An improved single-channel method to retrieve land surface temperature from the Landsat-8 thermal band," *Remote Sens.* **10**(3), 431 (2018).
22. Z. Qin, A. Karnieli, and P. Berliner, "A mono-window algorithm for retrieving land surface temperature from Landsat TM data and its application to the Israel-Egypt border region," *Int. J. Remote Sens.* **22**(18), 3719–3746 (2001).
23. F. Wang et al., "An improved mono-window algorithm for land surface temperature retrieval from Landsat 8 thermal infrared sensor data," *Remote Sens.* **7**(4), 4268–4289 (2015).
24. M. Isaya Ndossi and U. Avdan, "Application of open source coding technologies in the production of land surface temperature (LST) maps from Landsat: a PyQGIS plugin," *Remote Sens.* **8**(5), 413 (2016).
25. A. A. Lamaro et al., "Water surface temperature estimation from Landsat 7 ETM+ thermal infrared data using the generalized single-channel method: case study of Embalse del Río Tercero (Córdoba, Argentina)," *Adv. Space. Res.* **51**(3), 492–500 (2013).
26. J. Prats et al., "LakeSST: lake skin surface temperature in French inland water bodies for 1999–2016 from Landsat archives," *Earth. Syst. Sci. Data* **10**(2), 727–743 (2018).
27. Y. H. Kerr, J. P. Lagouarde, and J. Imbernon, "Accurate land surface temperature retrieval from AVHRR data with use of an improved split window algorithm," *Remote Sens. Environ.* **41**(2–3), 197–209 (1992).
28. USGS, "Landsat 8 OLI and TIRS Calibration Notices," https://www.usgs.gov/land-resources/nli/landsat/landsat-8-oli-and-tirs-calibration-notices (accessed 10 July 2019).
29. D. Reuter et al., "The Thermal Infrared Sensor (TIRS) on Landsat 8: design overview and pre-launch characterization," *Remote Sens.* **7**(1), 1135–1153 (2015).
30. A. Fadel and K. Slim, "Evaluation of the Physicochemical and Environmental Status of Qaraaoun Reservoir," in *The Litani River, Lebanon: An Assessment and Current Challenges*, pp. 71–86, Springer, Cham (2018).
31. A. Fadel et al., "First assessment of the ecological status of Karaoun Reservoir, Lebanon" *Lakes Reservoirs Res. Manage.* **19**(2), 142–157 (2014).
32. K. Slim et al., "Global warming as a driving factor for cyanobacterial blooms in Lake Karaoun, Lebanon," *Desalin. Water Treat.* **52**(10-12), 2094–2101 (2014).
33. A. Fadel et al., "Environmental factors associated with phytoplankton succession in a Mediterranean reservoir with a highly fluctuating water level," *Environ. Monit. Assess* **187**(10), 633 (2015).
34. A. Fadel et al., "On the successful use of a simplified model to simulate the succession of toxic cyanobacteria in a hypereutrophic reservoir with a highly fluctuating water level," *Environ. Sci. Pollut. Res.* **24**(26), 20934–20948 (2017).
35. J. A. Barsi, J. L. Barker, and J. R. Schott, "An atmospheric correction parameter calculator for a single thermal band earth-sensing instrument," in *Proc. IEEE Int. Geosci. and Remote Sens. Symp.*, vol. **5**, pp. 3014–3016 (2003).
36. V. García-Santos et al., "Comparison of three methods for estimating land surface temperature from landsat 8-tirs sensor data," *Remote Sens.* **10**(9), 1450 (2018).
37. X. Yu, X. Guo, and Z. Wu, "Land surface temperature retrieval from Landsat 8 TIRS—comparison between radiative transfer equation-based method, split window algorithm and single channel method," *Remote Sens.* **6**(10), 9829–9852 (2014).
38. J. C. Jiménez-Muñoz et al., "Revision of the single-channel algorithm for land surface temperature retrieval from Landsat thermal-infrared data," *IEEE. T. Geosci. Remote Sens.* **47**(1), 339–349 (2009).
39. J. C. Jiménez-Muñoz et al., "Land surface temperature retrieval methods from Landsat-8 thermal infrared sensor data," *IEEE. Geosci. Remote Sens. Lett.* **11**(10), 1840–1843 (2014).
40. P. Schneider and S. J. Hook, "Space observations of inland water bodies show rapid surface warming since 1985," *Geophys. Res. Lett.* **37**(22), 1–5 (2010).
41. M. Toffolon et al., "Prediction of surface temperature in lakes with different morphology using air temperature," *Limnol. Oceanogr.* **59**(6), 2185–2202 (2014).
42. H. Kettle et al., "Empirical modeling of summer lake surface temperatures in southwest Greenland," *Limnol. Oceanogr.* **49**(1), 271–282 (2004).

43. J. A. Sobrino et al., "Land surface temperature retrieval from LANDSAT TM 5," *Remote Sens. Environ.* **90**(4), 434–440 (2004).

44. S. K. McFeeters, "The use of the normalized difference water Index (NDWI) in the delineation of open water features," *Int. J. Remote Sens.* **17**(7), 1425–1432 (1996).

45. D. P. Dee et al., "The ERA-Interim reanalysis: configuration and performance of the data assimilation system," *Q. J. Roy. Meteor. Soc.* **137**(656), 553–597 (2011).

46. R. N. Simon, T. Tormos, and P-A. Danis, "Retrieving water surface temperature from archive LANDSAT thermal infrared data: application of the mono-channel atmospheric correction algorithm over two freshwater reservoirs," *Int. J. Appl. Earth Obs. Geoinf.* **30**, 247–250 (2014).

47. M. W. Becker and A. Daw, "Influence of lake morphology and clarity on water surface temperature as measured by EOS ASTER," *Remote Sens. Environ.* **99**(3), 288–294 (2005).

48. E. T. Crosman and J. D. Horel, "MODIS-derived surface temperature of the Great Salt Lake," *Remote Sens. Environ.* **113**(1), 73–81 (2009).

49. K. Schneider and W. Mauser, "Processing and accuracy of Landsat thematic mapper data for lake surface temperature measurement," *Int. J. Remote Sens.* **17**(11), 2027–2041 (1996).

50. E. S. Deutsch and I. Alameddine, "Hindcasting eutrophication and changes in temperature and storage volume in a semi-arid reservoir: a multi-decadal Landsat-based assessment," *Environ. Monit. Assess* **191**(1), 41 (2019).

51. E. Jeppesen et al., "Climate change effects on runoff, catchment phosphorus loading and lake ecological state, and potential adaptations," *J. Environ. Qual.* **38**(5), 1930–1941 (2009).

52. E. A. Stainsby et al., "Changes in the thermal stability of Lake Simcoe from 1980 to 2008," *J. Great. Lakes Res.* **37**, 55–62 (2011).

53. B. Vinçon-Leite et al., "Long-term temperature evolution in a deep sub-alpine lake, Lake Bourget, France: how a one-dimensional model improves its trend assessment," *Hydrobiologia* **731**(1), 49–64 (2014).

54. A. Fadel et al., "A simple modelling approach to simulate the effect of different climate scenarios on toxic cyanobacterial bloom in a eutrophic reservoir," *Ecohydrol. Hydrobiol.* **19**(3), 359–369 (2019)

55. C. E. Williamson et al., "Lakes and reservoirs as sentinels, integrators, and regulators of climate change," *Limnol. Oceanogr.* **54**(6part2), 2273–2282 (2009).

56. E. Moreno-Ostos et al., "Hydraulic management drives heat budgets and temperature trends in a mediterranean reservoir," *Int. Rev. Hydrobiol.* **93**(2), 131–147 (2008).

57. J. Blunden and D.S. Arndt, "State of the climate in 2015," *Bull. Am. Meteorol. Soc.* **97**(8), Si-S275 (2016).

58. I. Ostrovsky et al., "Long-term changes in the Lake Kinneret ecosystem: the effects of climate change and anthropogenic factors," in *Climatic Change and Global Warming of Inland Waters: Impacts and Mitigation for Ecosystems and Societies*, pp. 271–293, Wiley-Blackwell, Oxford (2013).

59. N. Sharaf et al., "Using Landsat and in situ data to map turbidity as a proxy of cyanobacteria in a hypereutrophic Mediterranean reservoir," *Ecol. Inf.* **50**, 197–206 (2019).

Biographies of the authors are not available.